LANGMUIR

pubs.acs.org/Langmuir Article

Mesoscale Aggregation of Sulfur-Rich Asphaltenes: *In Situ* Microscopy and Coarse-Grained Molecular Simulation

Christian B. Hammond,[⊥] Mohammadreza Aghaaminiha,[⊥] Sumit Sharma, Chongyang Shen, Hao Chen, and Lei Wu*

Cite This: https://doi.org/10.1021/acs.langmuir.2c00323 Read Online

ACCESS | Metrics & More | Article Recommendations | Supporting Information

ABSTRACT: Asphaltene aggregation is critical to many natural and industrial processes, from groundwater contamination and remediation to petroleum utilization. Despite extensive research in the past few decades, the fundamental process of sulfur-rich asphaltene aggregation still remains not fully understood. In this work, we have investigated the particle-by-particle growth of aggregates formed with sulfur-rich asphaltene by a combined approach of *in situ* microscopy and molecular simulation. The experimental results show that aggregates assembled from sulfur-rich asphaltene have morphologies with time-dependent structural self-similarity, and their growth rates are aligned with a crossover behavior between classic reaction-limited aggregation and diffusion-limited aggregation. Although the particle size distribution predicted using the Smoluchowski equation deviates from the observations at the initial stage, it provides a reasonable prediction of aggregate size distribution at the later stage, even if the observed cluster coalescence has an important effect on the corresponding cluster size distribution. The simulation results show that aliphatic sulfur exerts nonmonotonic effects on asphaltene nanoaggregate formation depending on the asphaltene molecular structure. Specifically, aliphatic sulfur has a profound effect on the structure of rod-like nanoaggregates, especially when asphaltene molecules have small aromatic cores. Interactions between aliphatic sulfur and the side chain of neighboring molecules account for the repulsive forces that largely explain the polydispersity in the nanoaggregates and corresponding colloidal aggregates. These results can improve our current understanding of the complex process of sulfur-rich asphaltene aggregation and sheds light on designing efficient crude oil utilization and remediation technologies.

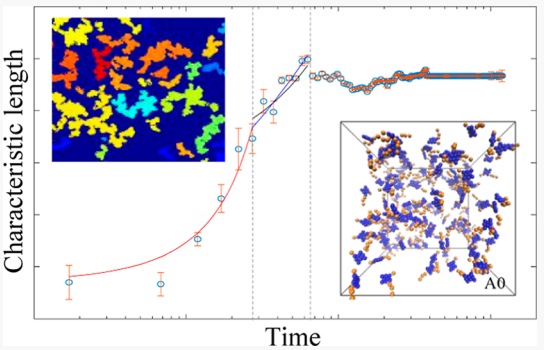

INTRODUCTION

Asphaltenes are one of the main components of crude oil and are known to have a high tendency to associate together to form aggregates that eventually cause fouling and clogging in the porous media of reservoirs and flow lines. Thus, asphaltene aggregation and precipitation have been extensively studied in the past few decades due to their importance in the oil industry.[1−23] By contrast, significantly less attention has been devoted to the environmental impacts of asphaltenes and their aggregates, which play important roles in the remediation of nonaqueous phase liquids (NAPLs), such as heavy fuel oil and coal-tar-contaminated aquifer.[10−14] Recent studies have shown that remediation strategies that result in the change in the solvation characteristics of the NAPLs could result in asphaltene aggregation, changing the wettability of the subsurface system, and hence, the distribution and recoverability of these contaminants.[10] As such, it is of great importance to both energy and environmental industry to understand the mechanisms that govern asphaltene aggregate formation.

Asphaltenes are a class of high-molecular-weight polar compounds that are defined by their insolubility in short-chain alkanes and contain both aliphatic and aromatic hydrocarbons, polar heteroatom-containing functional groups (*e.g.*, sulfur and nitrogen), and some trace metals.[15] Aggregation of asphaltene is an extremely complex process and has been studied extensively in the past few decades.[4,16−20] According to the widely adopted modified Yen−Mullins hierarchical model,[4] there are three length scale characteristics to asphaltene stability: (1) the individual asphaltene molecules (∼1.5 nm) have aromatic rings with substituted alkanes around their edge; (2) nanoaggregates and associated small clusters (∼30 nm) are formed by stacking of asphaltene molecules; and (3) large clusters of nanoaggregates (∼10 μm) are formed with a fractal structure. The Yen−Mullins model predicts that asphaltene molecules form small and dense nanoaggregates, which, in turn, aggregate loosely into large clusters. This model

Received: February 9, 2022
Revised: May 6, 2022

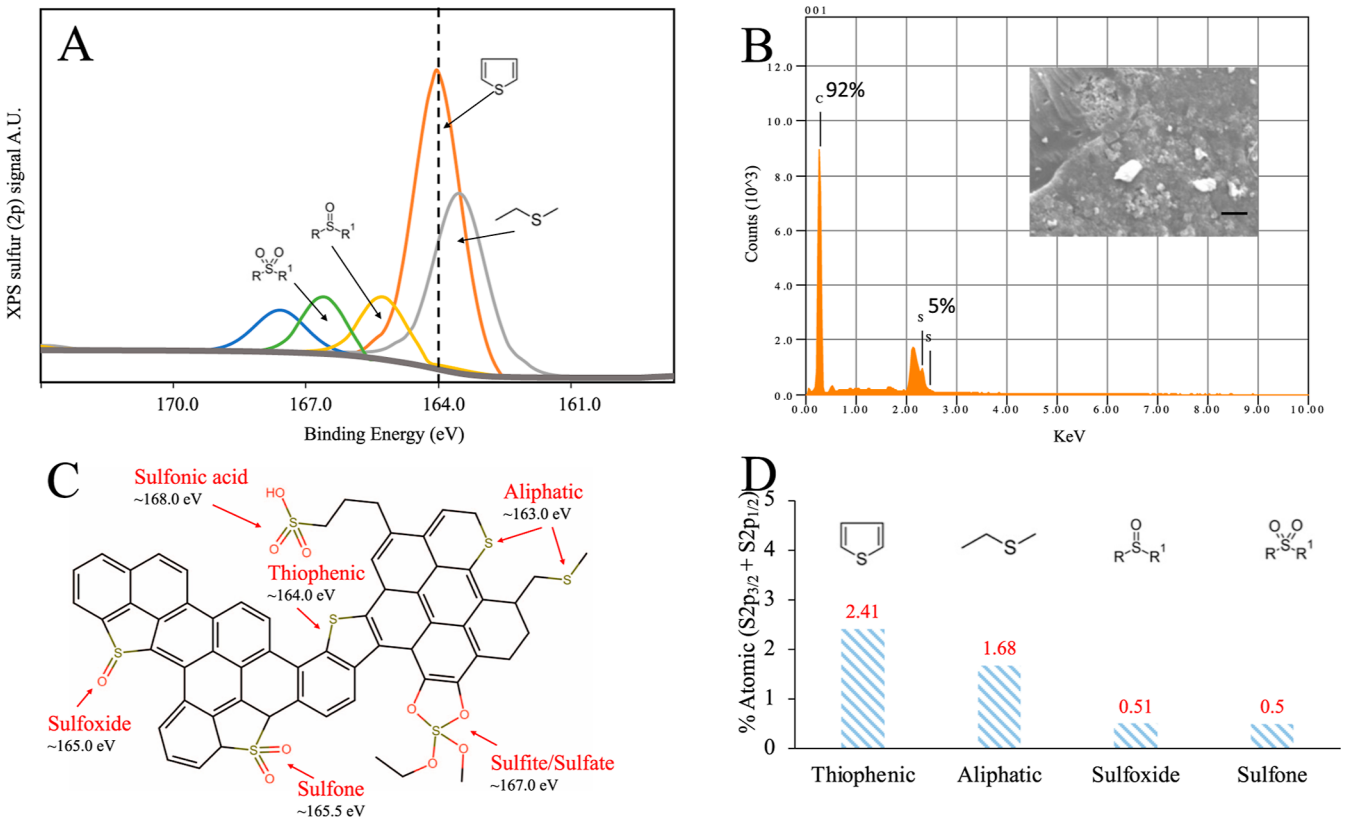

Figure 1. Sulfur characterization in asphaltenes. (A) XPS Sulphur 2p spectrum of the asphaltene sample analyzed in this study; (B) SEM−EDX analysis of the chemical composition of the asphaltene sample. Inset: zoom-in view of representative asphaltene particles in the dry sample. The scale bar represents 1 μm; (C) representative functionalities found in asphaltenes in the literature; (D) XPS S 2p signals in terms of atomic percentages for the analyzed asphaltene sample.

has received numerous experimental and theoretical support.[4,21−23] On the one hand, a variety of experimental methods have revealed the hierarchical asphaltene aggregation process. Small-angle neutron scattering (SANS) and small-angle X-ray scattering (SAXS) provide a robust method of measuring the size and shape of asphaltene nanoaggregates in both solvents and crude oils.[22,24,25] In these studies, shape-independent analyses yield nanoaggregates with a size ranging from 30 to 100 nm, depending on the crude oil, pretreatment, and analysis method. The SANS and SAXS data can be fitted to a number of shape and structure factors. However, because of the polydispersity of the nanoaggregates, these results should be taken with caution. More recently, *in situ* high-resolution microscopy, known for its nondestructive and noncontact features, has been used to directly observe the aggregation kinetics and the fractal nature of the network formed by asphaltene aggregates.[26,27] On the other hand, molecular simulations have been employed to study the molecular-level arrangement of asphaltenes in the aggregates.[19,28] All-atom molecular simulations have proven to be a useful tool to probe the formation of nanoaggregates predicted in the early stages of the Yen−Mullins assembly hierarchy at the level of molecular scale; however, the computational costs have limited these simulations to either shorter than 100 ns or fewer than 50 asphaltene molecules.[23] These constraints make it unfeasible to probe the clustering of asphaltene nanoaggregates during the late stage of the Yen−Mullins assembly hierarchy. Coarse-gained molecular simulations offer a means to access the time and length scales necessary to observe aggregates formation at the cluster level.[23,29,30] By combining coarse-grained molecular models parametrized on all-atom data, Wang and Ferguson[23] performed mesoscale simulations of aggregation of hundreds of asphaltenes over microsecond time scales. Their simulation results confirmed the three-stage asphaltene aggregation process described by the Yen−Mullins model.

Despite the extensive experimental and theoretical studies, questions still remain in terms of the description and interpretation of the fundamental details of asphaltene aggregation. Recently, researchers identified sulfur, a heteroatom in asphaltene molecules, plays an important role in asphaltene aggregates formation.[15] A molecular dynamics simulation study by Sodero *et al.*[20] showed that sulfur atoms grafted directly to the conjugated backbone (polyaromatic core) do not prevent aggregation, while the presence of sulfur atoms on the lateral chains has a pronounced effect on the aggregation due to steric hindrance and Coulomb repulsion between sulfur and nitrogen atoms of the adjacent molecules. Another recent experimental study by Zaluzec *et al.*[31] found that asphaltene with a high sulfur content can form dense consolidated nanoaggregate structures, while asphaltene with low levels of sulfur form interconnected network structures. The insights from these two studies have shown that sulfur has nontrivial effects on asphaltene stability at molecular and nanoaggregates scales. However, to date, the fundamental process of sulfur-rich asphaltene aggregation at the colloidal cluster level is not fully understood. This information is critical to developing solvation-based remediation techniques and mitigating the environmental impacts of sulfur-rich asphaltene in groundwater.

https://doi.org/10.1021/acs.langmuir.2c00323
Langmuir XXXX, XXX, XXX−XXX

Many studies have applied colloid aggregation principles to describe asphaltene aggregation kinetics at the large cluster scale.[16−18,21,26,27,32] According to Derjaguin−Landau−Verwey−Overbeek (DLVO) theory, asphaltene aggregation is driven by two main mechanisms: (1) diffusion-limited aggregation (DLA)[33] and (2) reaction-limited aggregation (RLA).[34] Each mechanism has different rate-limiting physics, aggregation dynamics, and cluster-mass distributions. The aforementioned studies highlight the effects of the sulfur content and position on asphaltene particle interactions. These interactions govern asphaltene nanoaggregate formation, which will ultimately affect the kinetics and morphology of micro-sized asphaltene aggregates. As such, the research objective is to quantify the growth kinetics and morphologies of aggregates formed from sulfur-rich asphaltene and elucidate the mechanisms governing this process.

Here, we aim to study sulfur-rich asphaltene aggregation on the mesoscale, wherein the nanoaggregates form the primary building blocks of larger aggregates. We first observed asphaltene aggregate growth kinetics while simultaneously observing their morphological evolution by using customized *in situ* microscopy. This is especially important for sulfur-rich asphaltene, where the relationship between kinetics and the structure remains poorly understood. The aggregate formation kinetics, colloidal structural evolution, and aggregate morphologies were examined by analyzing the growth curve, particle size distribution, and fractal structures, respectively. This analysis is based on advanced image processing algorithms, which allow for the examination of sulfur-rich asphaltene aggregation in detail. We then conducted coarse-grained molecular simulations to study the molecular-level structural evolution from nanoaggregates to large aggregate clusters and compared the results with the Yen−Mullins hierarchy model. Three prototype asphaltene models were used to study the effects of aliphatic sulfur on asphaltene aggregates formation. To the best of our knowledge, this study is one of *few* studies on mesoscale sulfur-rich asphaltene aggregation combining both *in situ* microscopy and coarse-grained molecular simulations.

EXPERIMENTAL SECTION

Experimental Methods. *Materials and Characterization.* The crude oil used in this project was obtained from Venezuela with an asphaltene content of 9.0 wt %. A detailed characterization of the extracted asphaltenes was conducted as follows: elemental analysis by an elemental analyzer (Vario macro cube, Elementar, Germany) and energy-dispersive X-ray spectroscopy (EDX) were utilized to determine the composition of asphaltenes. X-ray photoelectron spectroscopy [K-Alpha X-ray photoelectron spectrometer (XPS), Thermo Scientific, USA] was applied for the direct speciation and quantification of organic sulfur forms in the extracted asphaltenes. The results of these characterizations are shown in Table S1 and Figure 1. Toluene (>99%, Fisher Scientific Inc.) and *n*-heptane (>95%, Fisher Scientific Inc.) were used as the solvent and precipitant, respectively.

Preparations of Model Oil. The model oil was prepared by using the procedure described by Hoepfner *et al.*,[21] where asphaltene was first extracted from crude oil with a 40:1 heptane dilution, and the resulting mixture was stirred for 24 h before separating the precipitated asphaltenes from the crude oil/heptane solution by centrifugation. The solid asphaltenes were continuously washed with heptane to remove any trapped nonasphaltene components and dried in an oven at 70 °C to evaporate any residual heptane. The model oil was then prepared by dissolving the asphaltenes in toluene to achieve the target concentration of 1 wt %. The model oil was continuously stirred for 5 days to allow the asphaltene to fully dissolve. All samples were prepared and stored in glass vials with Teflon-lined caps. More details can be found elsewhere.[21]

Target Asphaltene Concentration and the Instantaneous Onset Point. Asphaltene aggregation kinetics and morphology depend on the initial asphaltene and precipitant concentrations. Previous studies have shown that at low concentrations (less than 1.5 wt % asphaltenes in the solvent), the asphaltene aggregate growth generally follows the Smoluchowski model, while at high concentrations, the aggregation mechanisms become more complex because the diffusivity coefficient is asphaltene concentration-dependent.[35] The instantaneous onset of precipitation of asphaltene in this study is mainly determined by the concentration of heptane (precipitant) that has to be added to the model oil (*i.e.*, asphaltene/toluene), where the first aggregates were observed by optical microscopy after less than 30 min of mixing with the precipitant. In the existing literature, the onset concentration for heptane depends on the origin and the concentration of asphaltenes and varies from 40 to 80 vol %. In this study, the concentration of *n*-heptane added to the model oil was varied, starting from 5 vol % until the defined instantaneous onset of precipitation was reached, and this concentration was measured to be 52 vol % heptane (Figure S1). As the first step in a series of studies to evaluate the effects of sulfur on the asphaltene aggregation process, a low concentration of 1.0 wt % asphaltene in toluene and a precipitant concentration of 55 vol % around the onset point were used in this work to examine sulfur-rich asphaltene aggregation behavior. To fully quantify the effect of asphaltene and/or the precipitant concentration on the aggregation of sulfur-rich asphaltene, a more comprehensive study needs to be performed, which is not the goal of this work.

In Situ Microscopy Experiments. The experiments to study asphaltene aggregation were conducted using a liquid cell mounted on a 100× magnification inverted optical microscope (Eclipse Ti-E, Nikon Instruments Inc. USA). The details of this liquid cell were described previously.[36,37] To induce aggregation, precipitant heptane was mixed to a model oil at a 55 vol % concentration. This ratio ensures that aggregates are formed. Then, 1 μL of a mixture of the model oil and precipitant was delivered to the cell, which was then sealed and mounted onto the stage of the microscope. This procedure typically took 1 min, so that the initiation of microscopy observations at $t = 0$ corresponds to 1 ± 0.5 min after mixing. Images with resolution ~0.07 μm were taken every 10 s until the aggregate growth saturated. At the end of the experiment, a large image that is 3×3 larger than the image with a normal field of view was taken and stitched together to collect larger statistics of the size and shape of mature aggregates under steady-state conditions. Particle size distributions and morphology measurements were obtained from the large stitched image.

Image Analysis. All analysis was performed in MATLAB, and the key steps are summarized here. First, background noise was subtracted from each image. Then, Otsu's thresholding method was used to obtain a binary image for the subsequent analysis of particle size evolution through time. The autocorrelation length was determined from a customized algorithm based on the fast Fourier transform, whereas the error was estimated using a bootstrap resampling method. The details of the autocorrelation algorithms were reported in a previous study[37] and provided in the Supporting Information S4. Briefly, a 2D spatial autocorrelation image of the microscopy image was firstly generated, and then the radially averaged distribution of the autocorrelation image was plotted, to which a simple exponential function was fitted to extract the characteristic length λ. It is worth noting that λ is proportional to the radius of each cluster r, measured by $\sqrt{A}$, where A is cluster area measurement determined by counting the number of pixels in each identified cluster and converting the measured pixels to real dimensions. Validation of the exponential fitting from our imaging and data acquisition system has shown that the lower limit of the size of aggregates, which can be identified from this study, is 0.9 μm (Figure S2). The steps involved in the processing of the large-stitched image are illustrated in Figure 2. In brief, after raw image data were extracted and stored, a global threshold using the Ostwald criterion was applied to generate the

https://doi.org/10.1021/acs.langmuir.2c00323
Langmuir XXXX, XXX, XXX−XXX

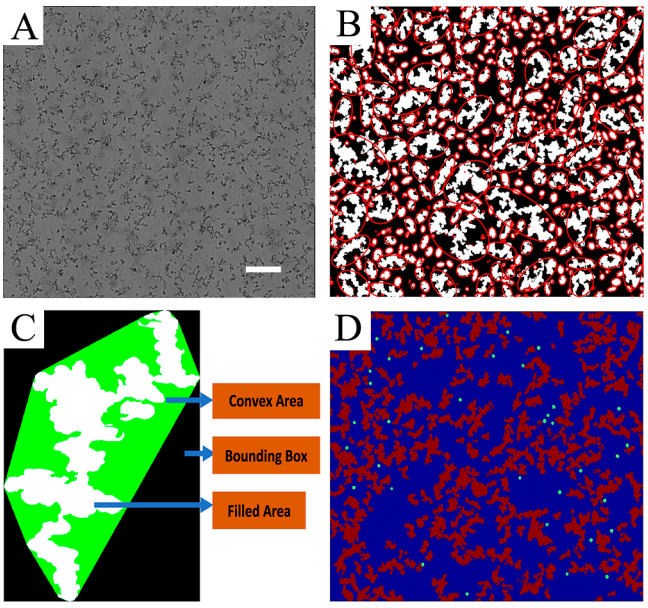

Figure 2. Processing of large-stitching images and identification of large and small aggregates at a colloidal cluster scale. (A) Original bright field large scan image of asphaltene aggregates which is 3 × 3 larger than the image with a normal field of view. (B) Identified particles (nanoaggregates) and aggregate clusters in the binary image after global threshold using the Ostwald criterion. The identified objects were determined by randomly labelling connected objects and filled with an elliptical shape. (C) Definitions of cluster properties. Filled-Area: actual number of pixels in the region; bounding-box: the smallest rectangle containing the region; convex-area: the smallest convex polygon containing the region; eccentricity: the ratio of the distance between the foci and ellipse and its major axis length; solidity: area/convex-area; solidity2: filled-area/bounding-box; and solidity-ellipse: filled-area/best fit ellipse. (D) Identified small clusters (white) and large clusters (red). Details of criteria are shown in Figure S2. Scale bar represents 30 μm.

binary images. Image segmentation was used to identify all objects, and the objects were characterized using the MATLAB regionprops function and best fit with ellipses. Four morphology parameters were defined and calculated to identify individual particles (nanoaggregates), small and large aggregate clusters: area, solidity, solidity-ellipse, and eccentricity. Details of the definitions and acceptance criteria used in this study are illustrated in Figure S3. Fractal dimensions of aggregates (d_f) were computed by the following relationship: $A = R_g^{d_f}$ where R_g is the radius of gyration. In this study, R_g was calculated as

$$R_g = \sqrt{(x - x_c)^2 + (y - y_c)^2/(N - 1)} \quad (1)$$

where x_c and y_c are the x–y coordinates of the centroid of each cluster, x and y are the x–y coordinates of each pixel in a cluster, and N is the number of pixels in each cluster. Also, very large clusters are more likely to intersect the boundary of the image than small ones, so the image analysis could be artificially deficient in large clusters.

Computational Methods. *Simulation Procedure.* The major sulfur species in the asphaltenes used in the experimental studies include thiophenic sulfur and aliphatic sulfur. A previous study has shown that thiophenic sulfur has little influence on the aggregation behavior of dimer and trimer asphaltene systems, and aromatic rings with sulfur might not be differentiated fron those without sulfur.[20] In contrast, aliphatic sulfur has a more sensitive effect on the stabilities of these systems. Furthermore, the potential of mean force (PMF) curves between all-atom and coarse-grained models have shown that sulfur on the aliphatic chain can be replaced by the C atom in the first-order approximation.[23] Thus, for the simplicity of simulation, we have focused on studying the effects of aliphatic sulfur on the asphaltene aggregate structure by employing molecular simulations using asphaltene with different aromatic core and aliphatic side chains. For this purpose, we have chosen to study three representative asphaltene molecular models, the same as the ones previously studied by Wang and Ferguson.[23] (Figure 3). A0 comprises a core of 8 fused aromatic rings, bound to one long side chain $C_8H_{17}S$ and one short side chain C_3H_7, and has a molecular weight of 540 g/mol. A1 has the same side chains as A0 but possesses a larger aromatic core comprising 12 fused aromatic rings, while A2 has the aromatic core identical to A1 but is bound to three long side chains: two $C_{12}H_{25}$ and one $C_{11}H_{23}S$. Therefore, differences in the aggregation tendency between A0 and A1 will highlight the role of the aromatic core, whereas those between A1 and A2 will elucidate the effect of the side chains. Each of these asphaltene structures contains one sulfur atom, which can be represented by the aliphatic chain (a) in Figure 3. A0 has a sulfur content of 5.92% by weight, which is comparable to that measured in the asphaltene sample used in our experiments. The molecular weight and corresponding sulfur content of A1 and A2 are 648, 985 g/mol, 4.9% w.t., and 3.2% w.t., respectively.

Following the approach of Wang and Ferguson,[23] we employed the coarse-grained (CG) Wet Martini force field (v2.2)[29] to model/parametrize toluene and *n*-heptane solvents and the three asphaltene molecules. The topologies of the asphaltene molecules under Martini mapping are displayed in Figure 3. More details on the coarse-graining approach can be found elsewhere.[23] We then performed simulations of the assembly of these three asphaltene molecules in an *n*-heptane solvent at a concentration of approximately 15% w.t. Periodic boundary conditions were applied in all the three directions of the simulation box. In all the simulations, the box size was 15.6 × 15.6 × 15.6 nm^3, and the total number of molecules in each system is shown in Table S2, Supporting Information. It should be noted that this initial concentration is larger than used in our experiments, and this choice is justified as follows: (1) simulating the system at an experimental concentration would require 100 asphaltene molecules in 10^7 heptane/toluene molecules in an approximately 100 × 100 × 100 nm^3 box, which is intractably large for a simulation study; (2) at a low concentration, the aggregation kinetics are slow, which makes the simulations computationally expensive; and (3) our primary focus is to understand the effects of aliphatic chains on the morphology of aggregates formed by the different asphaltene molecules. Thus, conducting simulations at a higher concentration significantly improves the computational efficiency by reducing the diffusion time while enabling direct observations of the formation of large aggregates.

The parameters of the simulation system were chosen to be the same as in the previous work done to parameterize the asphaltene model on the Martini force field.[23] A spherical cut-off of 1.4 nm was chosen for the Lennard Jones (LJ) interactions. Coulombic interactions were modeled using Reaction-Field-zero (RF-zero) with a spherical cut-off of 1.4 nm. The relative dielectric constant was taken as 2.5. Both LJ and Coulombic interactions were smoothly shifted to zero beyond the cut-off. The Bussi *et al.*[38] velocity-rescaling thermostat and the Parrinello–Rahman barostat were used with the coupling time constant of 12 ps. The isothermal compressibility and reference pressure were set to 1.175 × 10^{-4} bar^{-1} and 1.0 bar, respectively. All simulations were performed on GROMACS/5.1.2 molecular simulation package,[39] and the results were postprocessed using Python. The initial configuration of the system was energy minimized by employing the steepest descent algorithm with the maximum force tolerance of 1000.0 kJ mol^{-1} nm^{-1}. This was followed by a 25 ns canonical ensemble (constant number of particles N, volume V, and temperature T) simulation with a 10 fs timestep for pre-equilibration. Then, three independent 1 μs isothermal-isobaric (constant N, pressure P, T) ensemble simulations with a 10 fs timestep were performed, similar to the previous studies,[23,40,41] and the data was collected for the last 0.5 μs for all the simulations. All the simulations are performed at 300 K. In addition to studying the aggregation of A0–A2, we also performed molecular simulations of the aromatic cores of A0 and A1 in the absence of the aliphatic side

https://doi.org/10.1021/acs.langmuir.2c00323
Langmuir XXXX, XXX, XXX–XXX

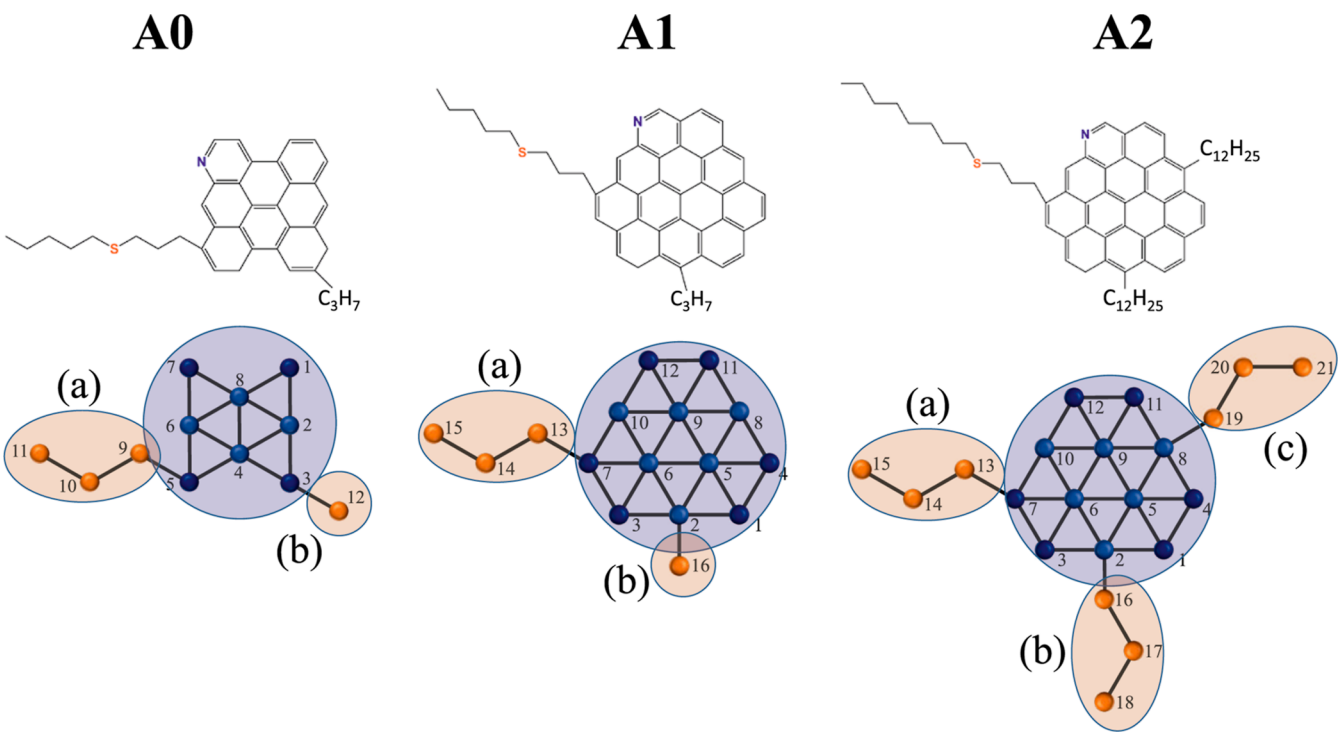

Figure 3. Topologies of asphaltene molecules and their Martini force field mapping.[23] Adapted in part with permission from [Wang, J.; Ferguson, A. L., Mesoscale Simulation of Asphaltene Aggregation. *The Journal of Physical Chemistry B* 2016, *120* (32), 8016−8035]. Copyright [2016] [American Chemical Society]. Molecular weights: A0: 540 g/mol, A1: 648 g/mol, A2: 985 g/mol. In the coarse-grained (CG) representations, we employed 3 types of beads: C1—representing aliphatic side chains (orange); M—representing aromatic rings with partial charge +q (dark blue); and M—representing aromatic rings with partial charge −q (light blue). Please note: the aliphatic chain labeled as (a) in A0−A2 reflects the aliphatic chain, which includes one aliphatic sulfur for each asphaltene molecule.

chains for comparison. These simulations were performed with the same methodology as described above. A correlation between MD configurations can be determined by calculating the autocorrelation function for the slowest dynamics of a system. We found that the slowest dynamics correspond to the aggregation of asphaltene molecules. The longest correlation length was found to be 0.5 μs. We note that our equilibration timescales are at least 10 times larger than the correlation length. Furthermore, the production runs are sufficiently long to provide a good statistical description of the molecular configurations of the systems.

Structural Metrics of Asphaltene Aggregates. The radial distribution function, $g(r)$, between the aromatic cores, aromatic cores and the side chains, and between the side chains was calculated to examine the structure of the aggregates. Fractal dimensions of the assembled aggregates of asphaltene molecules were found to determine the morphology of the aggregates. From the molecular simulation trajectories, the correlation sum, $C(\epsilon)$, is calculated as[23]

$$C(\epsilon) = \frac{1}{N(N+1)} \sum_{i,j=1,i\neq j}^{N} H(\epsilon - r_{ij}^{\mathrm{COM}}) \quad (2)$$

where N is the number of asphaltene molecules in the system, H is the Heaviside step function, r_{ij}^{COM} is the center of mass distance between the molecules i and j, and ϵ is the cutoff distance. $C(\epsilon)$ identifies the fraction of molecular pairs that are within a distance of ϵ. The fractal dimension d_f is determined by fitting the relationship $C(\epsilon) \sim \epsilon^{d_f}$.[36] Following the approach of Wang and Ferguson,[23] we estimated d_f for two regions (I and 2) by computing the slope of the least square fit to the log−log plot of $C(\epsilon)$ in each region. To further characterize the asphaltene aggregates, we performed a cluster analysis to identify the size distribution of the aggregates. Two asphaltene molecules were assigned to the same cluster if the distance between the center of mass of their aromatic cores was less than 0.55 nm. This threshold is an average of the first peak of the aromatic−aromatic $g(r)$ of A0, A1, and A2 molecules of the three systems. The ensemble average of the number of molecules belonging to clusters of different sizes is reported, which we refer to as "frequency".

RESULTS AND DISCUSSION

Asphaltene Characterization. The results of the elemental analysis show a total heteroatom (nitrogen, sulfur, and oxygen) content of approximately 10 wt %, which is consistent with the previous studies.[15] The sulfur content from both bulk and surface measurements was determined to be as high as 5.67 wt %, which is considered sulfur-rich based on sulfur content (0−8 wt % range) reported in the existing literature (Table S1).[42,43] The sulfur content determined from XPS and EDX analysis (Figure 1B) is slightly higher than that from the elemental analysis, which is likely attributed to the presence of sulfur linkage (an aliphatic chain) that stabilizes the aromatic rings in asphaltenes.[42] Figure 1 shows the results of qualitative and quantitative analysis of sulfur forms determined from the XPS sulfur 2p signal. The results show that the dominant species in asphaltenes are thiophenic sulfur (∼164 eV) in the aromatic rings, followed by aliphatic sulfur (∼163 eV) in the side chains. This was previously observed for other heavy petroleum samples and interpreted in the light of available model asphaltene compound results.[44,45] A small number of oxidized forms of sulfur, including sulfoxides and sulfones in thiophenic environments, is also observed in the asphaltene sample (Figure 1A,D), likely due to the oxidation of thiophenic sulfur when exposed to air, as reported in the literature.[15] It is worth noting that the characterization of oxidized forms of sulfur by XPS is complex; thus, some oxidized species have not yet been well-addressed. For

https://doi.org/10.1021/acs.langmuir.2c00323
Langmuir XXXX, XXX, XXX−XXX

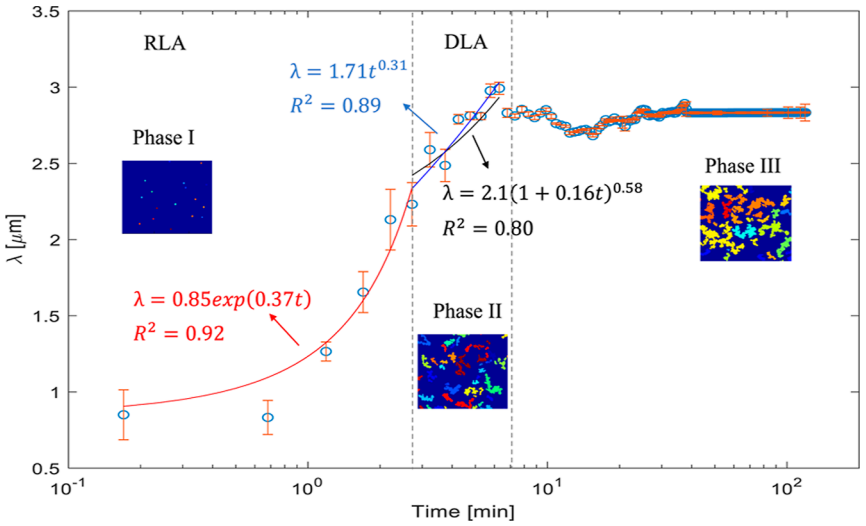

Figure 4. Characteristic length (λ) of clusters as a function of time. A bootstrap method was used to evaluate the error of experimental data. The insets show representative particle/cluster morphologies at various phases. Experimental growth data in phases I and II were also fitted with RLA and DLA kinetics, respectively. Red and black lines represent the best fit curves for RLA kinetics: $r = r_0 \exp(t/\tau_r d_f)$ and DLA kinetics: $r = r_0(1 + t/\tau_r)^{1/d_f}$, respectively. The values of d_f for RLA and DLA are 1.99 and 1.73, respectively, and determined by morphological analysis. The blue line represents the best fit curve for the simplified Smoluchowski kinetics: $\langle r \rangle = kt^{\beta}$, where β is the growth exponent. The details (goodness of fit) of least-squares fitting are shown in Table S3.

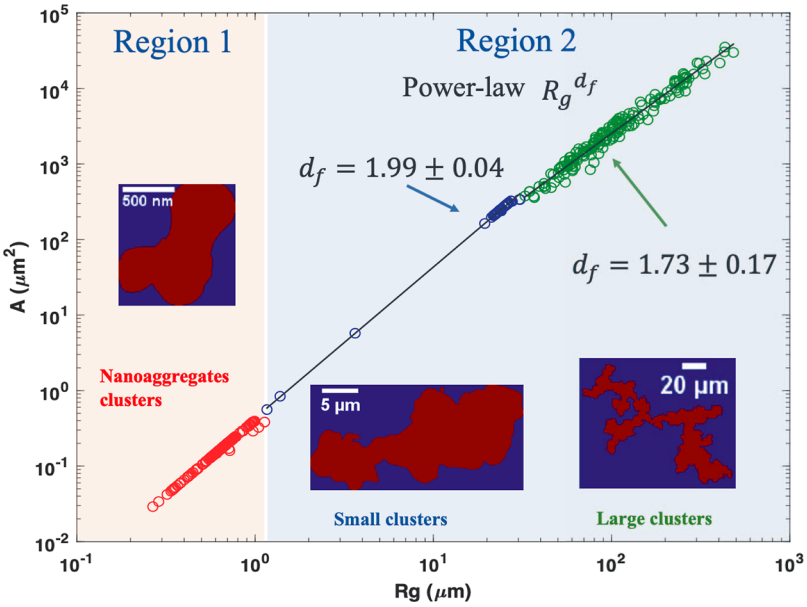

Figure 5. Integrated log−log plot of average area A as a function of the radius of gyration R_g between region 1 and region 2. Particles in region 1 represent the primary particles observed at the beginning of microscopy observations. According to the Yen−Mullins hierarchical model,[4] these primary particles are asphaltene nanoaggregates/clusters. Data in region 2 show best-fit two scaling regimes, indicating small clusters have RLA-like structure ($d_f = 1.99 \pm 0.04$) while large clusters have DLA-like structure ($d_f = 1.73 \pm 0.17$). Primary particles were excluded from regression for colloidal fractal dimensions.

instance, the signal between 167 and 168 eV (the blue peak in Figure 1A) can be assigned to a variety of functionalities, such as thiosulfates, ester sulfate, organic sulfites, or sulphones in different polymeric materials.[45−48]

***In Situ* Microscopy of Asphaltene Aggregation.** *Aggregate Growth Curve.* The characteristic length λ determined from the autocorrelation function was used to examine the aggregation kinetics of sulfur-rich asphaltene. Figure 4 shows the growth of the average cluster/aggregate size λ as a function of time. We observed a significantly slow aggregation period preceding the onset of fast aggregation (phase I). At this stage, we verified that these particles (referred to as asphaltene nanoaggregates/clusters in the Yen−Mullins model) were undergoing Brownian motion; however, they collided with and separated from neighboring particles multiple times and correspond to the RLA process. During the next growth period (phase II), we observed that the aggregate size increased almost linearly over time on a semi-log plot, which is an indication of the DLA process. In the late stage (phase III), the characteristic length λ increased by ∼200%, in good agreement with prior studies,[24] and reached a saturated value due to a finite supply of particles. For classic RLA, the

https://doi.org/10.1021/acs.langmuir.2c00323
Langmuir XXXX, XXX, XXX−XXX

characteristic aggregate size grows with time as $\lambda = \lambda_0 \exp(t/\tau_R d_f)$,[27] where τ_R is the characteristic reaction time, and d_f is the fractal dimension of aggregates formed during the RLA process. In order to test whether the RLA model can be used to describe the slow aggregation behavior we observed in this study, we fit the experimental data points in phase I to the above relation by using the d_f determined from the aggregate morphological analysis. Specifically, the 2-D d_f of aggregate clusters during RLA is 1.99 ± 0.04 (Figure 5). The best fit τ_R was found to be 1.4 ± 0.15 min with $R^2 = 0.92$. For the classic DLA, the particle growth can be described by the following relation: $\lambda = \lambda_0(1 + t/\tau_D)^{1/d_f}$,[27] where τ_D is the characteristic diffusion time. Similarly, we fit the experimental data points in Phase II to the DLA relation and got the best fit τ_D of 6.25 ± 0.11 min with $R^2 = 0.80$. More details on the goodness of fit are shown in Table S3. Apparently, both characteristic reaction time and diffusion time were consistent with our experimental observations. The characteristic diffusion time is larger than the reaction time, indicating that aggregation kinetics of sulfur-rich asphaltene is dominated by DLA despite the short RLA process at the initial stage. Furthermore, previous studies have found that the growth rate of the average aggregate cluster size can be directly related to the scaling properties of the diffusion coefficient of individual clusters when the growth process is dominated by cluster diffusion and coalescence. Moreover, the scaling exponent of the 2D cluster due to the Brownian diffusion was found to be 1/2, yielding a predicted aggregate growth exponent of 1/3.[49] This result is in good agreement with the growth exponent (0.31 ± 0.11) we obtained in our experiment, indicating the sulfur-rich asphaltene aggregation observed in our study is dominated by cluster diffusion and coalescence.

In the existing literature, the crossover between RLA and DLA for asphaltene aggregation has also been reported. Yudin *et al.*[18] observed that when the asphaltene concentration is above the critical micelle concentration, the RLA process dominates at the initial stage of the aggregation process, and then the aggregation mechanism transitions to DLA at longer times and increasing sizes. However, whether this crossover kinetics between RLA and DLA can be predicted by a universal description remains unclear since a few characteristics determined from their system deviate from the results in our study. There are several physical effects that could cause the above discrepancy, including the high content of sulfur detected in our asphaltene sample; however, more investigations are needed to further examine how sulfur affects asphaltene aggregates formation. Nevertheless, the results we have presented above provide a useful characterization of the sulfur-rich asphaltene aggregate growth. Although the dominant experimental growth exponent is consistent with Smoluchowski growth kinetics, the growth curve has shown that their aggregation behavior follows a crossover between RLA and DLA. Specifically, in the early stage of aggregation, during a regime of a slow cluster growth, the aggregation kinetics resemble that of RLA; however, during the latter, rapid growth stage, the aggregation kinetics become compatible with expectations for DLA. Given a piece of compelling evidence in a recent simulation study that sulfur atoms in the middle of the aliphatic chain and a chain end have an important effect on the stability of both asphaltene dimers and trimers due to both steric hindrance and Coulomb repulsion,[20] a possible explanation of the slow cluster observed in the early stage in this study could be attributed the aliphatic sulfur, one of the dominant sulfur species measured in our asphaltene sample.

Aggregate Morphology. We determined the morphological properties of the aggregates from the image mosaics at the end of the experiment, with a representative plot shown in Figure 5. The smallest clusters found in this sample are in the range of 100−150 μm^2, whereas the biggest clusters are 50,000 μm^2, suggesting that the clusters in the final stage of aggregation have a high degree of polydispersity.[50] The loose network morphology of sulfur-rich asphaltene aggregates disappears and changes to a denser isolated network, but the fractal character is still present. To illustrate this scale-invariant nature of aggregates, the fractal dimension of aggregates (d_f) was computed by the following scaling law between their area and the radius of gyration: $A \propto R_g^{d_f}$. This relationship assumes that in the asymptotic limit, R_g is linearly proportional to the total cluster size. Figure 5 shows a typical double-logarithmic plot of $A \propto R_g^{d_f}$. The scale invariance of clusters is evident over nearly 2 orders of magnitude of A. Figure 5 represents the best fit linear variations to both small and large clusters. The former evidently departs from the asymptotic scale invariance of the latter, indicating smaller clusters being more compact than the larger ones. The 2-D fractal dimension of small clusters in this study is 1.99 ± 0.04, suggesting that small aggregates formed from sulfur-rich asphaltene possess a dense morphology, which could be the consequence of the aggregation of compact sulfur-rich asphaltene nanoaggregates reported in prior studies.[31] This result could also be attributed to the effects of short-range repulsions from aliphatic sulfur or restructuring of clusters, which could result in more compact structures at small length scales.[45] The fractal dimension of large clusters was determined to be 1.73 ± 0.17, which is in accord with the structural characteristic of two-dimensional DLA. In the existing literature, a range of aggregate structures is evidenced by experimental studies revealing fractal dimensions of asphaltene aggregates varying over a range of 1.3−2.3 depending on temperature, pressure, and other experimental conditions.[21,32,51−54] However, none of these studies has included detailed characterization of sulfur species in their asphaltene samples, nor specific discussion of sulfur chemistry dependent-aggregate structures; thus, sulfur effects on asphaltene fractal aggregates at large cluster level still remain largely unknown.

It is also worth noting that according to the classic colloid aggregation theory, primary particles are ideal solid spherical particles and cannot be considered fractal structures. Previous studies have shown that including primary particles in power-law fits of *A versus* R_g limits the useful scaling range.[52,55] In order to ensure that polydispersity in primary particles does not contaminate the results, we excluded those primary building blocks from the regression used to determine the fractal dimension of the colloidal clusters. However, it must be highlighted that the primary particles shown in Figure 5 are actually asphaltene nanoaggregates, which are demonstrated to start revealing fractal properties at an average size of 7−8 asphaltene molecules.[56] Thus, we also evaluated the fractal dimensions of these nanoaggregates by a double-logarithmic plot of $A \propto R_g^{d_f}$ (Figure S4) as a comparison to the simulation results discussed in the later section. Our experimental measurements show that these nanoaggregates/clusters are compact objects with a Gaussian particle size distribution

https://doi.org/10.1021/acs.langmuir.2c00323
Langmuir XXXX, XXX, XXX−XXX

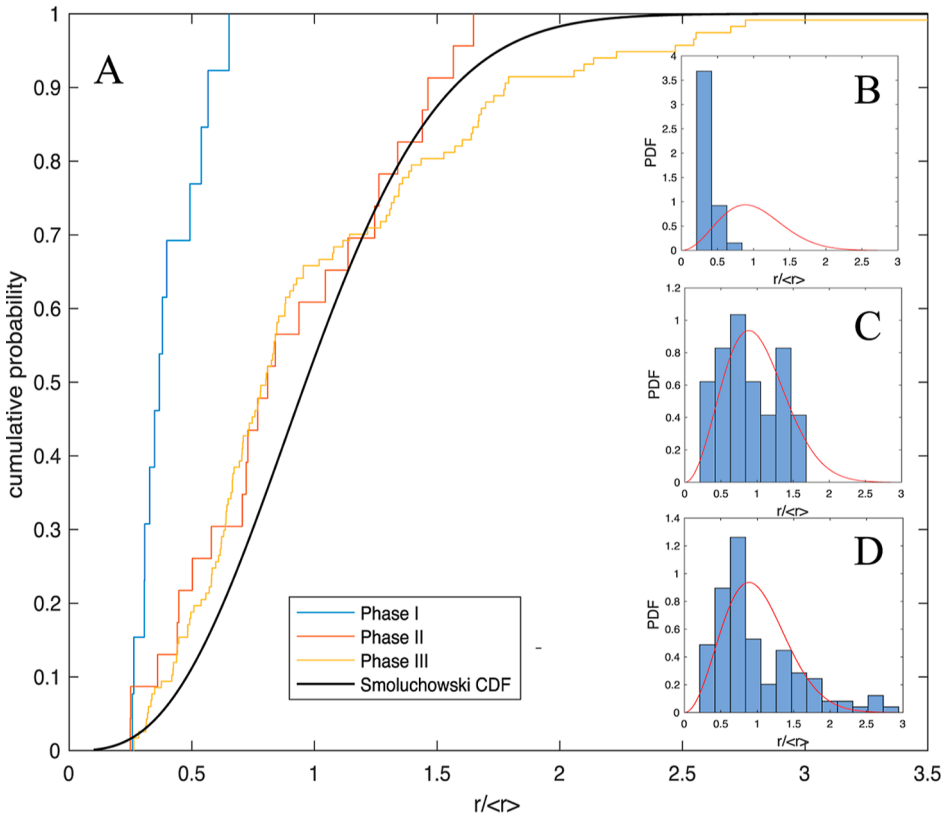

Figure 6. Cluster size distribution at different phases and comparison with the theoretical Smoluchowski particle size distribution. Cluster size distribution normalized by the mean size of asphaltene aggregates at the end of the experiment. (A) cumulative size distribution from phase I to III. The solid black line is the cumulative probability of the Smoluchowski particle size distribution using eqs 1 and 2 with $\sigma = 1/2$. (B–D) represent the probability density function (PDF) of the size distribution at phases I, II, and III, respectively. The red lines are the PDFs of the Smoluchowski particle size distribution mentioned above.

(Figure S5). The internal structure of these nanoaggregates is discussed in the molecular simulation section.

Aggregate Size Distributions. Given that the growth kinetics are also embodied in the cluster size distribution at the different growth stages, we also present measurements of cluster size distribution and its time dependence. The cumulative cluster size distribution (from phase I to III) is normalized by its mean value $r/\langle r\rangle$ to facilitate a direct comparison with theoretical predictions (Figure 6). According to Smoluchowski kinetics, a classical model that describes the time evolution of an ensemble of particles as they aggregate, a characteristic analytical solution for particle size distribution in the long-time limit can be written as[49,57]

$$F(\varphi) = \frac{2W}{\Gamma(\sigma+1)}(W\varphi)^{2a+1}e^{-(W\varphi)^2} \tag{3}$$

$$W = (\sigma+1)\frac{\Gamma(\sigma+3/2)}{\Gamma(\sigma+2)} \tag{4}$$

where $F(\varphi)$ is the analytical particle size distribution scaled to the average particle size, $\varphi = r/\langle r\rangle$, Γ is the standard Gamma function, and σ is the scaling exponent for particle/cluster diffusion. As discussed in the growth curve section, we used $\sigma = 1/2$ for 2D Brownian clusters. Figure 6 shows that at the initial stage of aggregation (phase I), the cluster size is significantly smaller than the mean and decays monotonically with the cluster size (asymmetric narrow distribution in Figure 6B), indicating that the number of small clusters decreases slowly due to reaction-limited aggregation. Experimental cluster sizes in phases II and III are in a reasonable agreement with the Smoluchowski model predictions (well-defined peaks in Figure 6C,D), except that the cluster size in phase III is slightly skewed to the right of the mean at the later stage of aggregation (large tail in Figure 6D). This indicates that when larger clusters have formed, the number of clusters decreases more rapidly. These results are also consistent with what we determined from the aggregate growth curve. The Smoluchowski model, which is ideal for DLA, underestimates the number of clusters that are smaller than the mean, while slightly overestimating the number of clusters that are larger than the mean. The crossover between RLA and DLA may explain this deviation between the theoretical predictions and our observations. In the RLA regime, where σ is apparently smaller than 1/2, the theoretical bell shape PSD curve would become left-skewed, while in the DLA regime, σ is close to 1/2, the feature of the crossover behavior would be less evident. In addition, the population of large clusters is slightly lower than that predicted by DLA, indicating that the classic cluster–cluster collision is not the only mode for aggregate growth. Our direct observations indeed show nonclassical growth mechanisms, such as particle-cluster aggregation and late-stage cluster coalescence, which also occur in the DLA-like aggregation regime, affecting the corresponding cluster size distribution. Despite these discrepancies, DLA is the dominant mode for large aggregate formation, while the Smoluchowski model provides a reasonable approximation of the size distribution of aggregates formed from sulfur-rich asphaltenes at the later stage.

https://doi.org/10.1021/acs.langmuir.2c00323
Langmuir XXXX, XXX, XXX–XXX

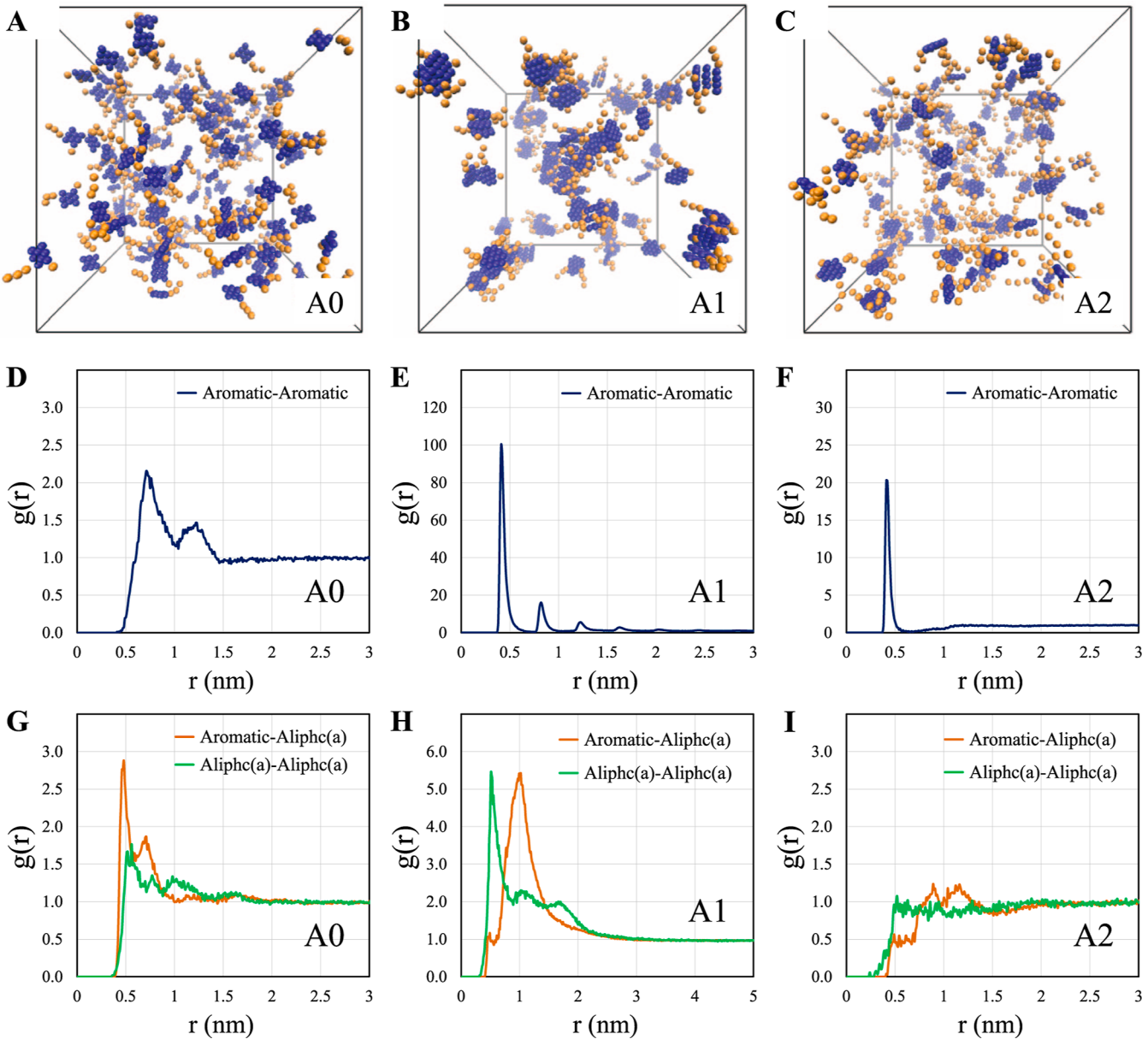

Figure 7. Snapshots of our MD simulations in equilibrium for (A) A0, (B) A1, and (C) A2 asphaltene molecules dissolved in a mixture of toluene and *n*-heptane. Radial distribution functions $g(r)$ between the aromatic cores of asphaltene types (D) A0, (E) A1, and (F) A2 are shown. The $g(r)$ between the aromatic core and aliphatic side chains (a) and between the aliphatic side chains (a) for (G) A0, (H) A1, and (I) A2 are also shown. In all the simulations, the asphaltene mass fraction with respect to toluene is 15 wt % and T = 300 K.

Mesoscale Simulation of Asphaltene Aggregation. *Internal Structure of Aggregates.* Figure 7A–C shows snapshots of the simulation system with the aggregates formed by the three types of asphaltene molecules, A0–A2, respectively. The corresponding radial distribution functions, $g(r)$ between the aromatic cores are plotted in Figure 7D–F. A0 shows some aggregation because of the small aromatic core. In contrast, A1 has significantly more aggregation, as shown by a much larger first peak in the $g(r)$. The aggregation in A2 is in between that observed for A0 and A1. Figure 7G–I shows the $g(r)$ between the center of masses of aromatic core and aliphatic chain and between the aliphatic chains. We have only considered the aliphatic chain labeled as (a) in Figure 3 since it reflects the aliphatic chain, which includes one aliphatic sulfur. Figure 7G, in conjunction with Figure 7D, shows that in the case of A0, there is no preferential aromatic stacking as the aromatic–aliphatic $g(r)$ is comparable to the aromatic–aromatic g(r). On the other hand, in the case of A1, there is a significant aromatic stacking. It is observed that aromatic–aliphatic $g(r)$ shows the first peak shifted to 1 nm (Figure 7H). In the case of A2, the aromatic–aliphatic and aliphatic–aliphatic $g(r)$ do not show any peaks, indicating that the aggregation is dominated by aromatic stacking (Figure 7I). These results indicate that aromatic stacking plays a dominant role in the formation of rod-like nanoaggregates of asphaltene molecules when the aromatic core is sufficiently large.

To further delineate the role of the aromatic core and the aliphatic side chains in the aggregation process, we simulated the A0 and A1 aromatic cores without the side chains (Figure S6, Supporting Information and Figure 8D–F), and the results are quite revealing. In the case of A0, the obtained $g(r)$ is similar, indicating that the aggregation did not change when

https://doi.org/10.1021/acs.langmuir.2c00323
Langmuir XXXX, XXX, XXX–XXX

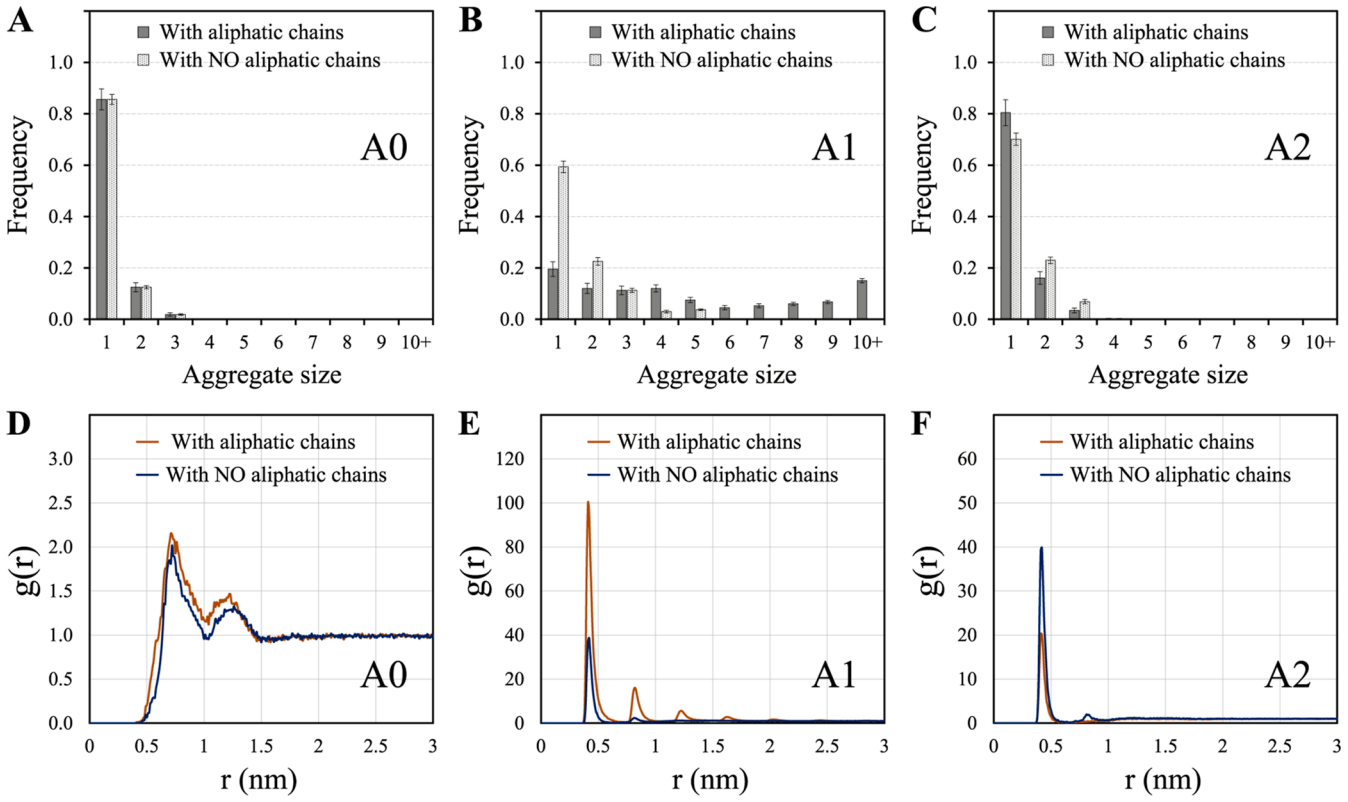

Figure 8. Distribution of aggregate sizes in (A) A0, (B) A1, and (C) A2. The aggregate size is defined as the number of molecules comprising the aggregate. The frequency on the *y*-axis represents the number of molecules in each aggregate size, that is, an aggregate of *n* molecules will be counted as n. The distribution of aggregates sizes in the absence of aliphatic chains is also shown for comparison. The aromatic−aromatic $g(r)$ for (D) A0, (E) A1, and (F) A2 is compared when only the A0 and A1 aromatic cores are simulated (aromatic cores of A1 and A2 are the same).

the chains were removed. This is understandable as the A0 aromatic cores are small that they only have a weak tendency to aggregate. On the other hand, the removal of aliphatic chains resulted in a decrease in the aggregation tendency of A1. Therefore, in the case of A1, the aliphatic chains facilitate aggregation probably by eliminating the nonspecific interactions between the aromatic cores that may occur in the absence of these chains. In the absence of the side chains, the aromatic cores may aggregate sideways, which may disrupt their aromatic stacking. On the other hand, in the presence of the side chains, the only way the asphaltene molecules can aggregate is *via* aromatic stacking. However, the aggregation of the A1 aromatic core in the absence of the aliphatic chains is still higher than the aggregation of A2 (with the chains). Therefore, in the case of A2, the aliphatic chains hinder aggregation. This result can be understood as follows: in the case of A1, the aromatic stacking can occur without steric hindrance between the aliphatic chains. However, in the case of A2, aromatic stacking also results in steric hindrance between the three aliphatic chains around the aromatic core. Figure 8A−C compares the aggregate size distribution in A0, A1, and A2 with and without the aliphatic chains. It is observed that A0 molecules form small aggregates. A1 displays a much larger aggregate size distribution and forms large aggregates. Clearly, when the aliphatic chains are removed, only smaller aggregates are formed. A2 shows a smaller aggregation tendency than A1 and thus forms smaller aggregates. This analysis reveals that the role of aliphatic side chains in the aggregation behavior of asphaltenes is nonmonotonic and richer than previously thought.

Fractal Dimension of the Aggregates. We present log−log plots of the correlation sum $C(\epsilon)$ computed from the equilibrium morphology of asphaltene architectures A0, A1, and A2 over several orders of magnitude of correlation sphere diameter ϵ in both 2-dimensional (Figure 9) and 3-dimensional systems (Figure S7). This allows us to reveal fractal dimensions of simulated asphaltene aggregates from nano- to micro-cluster scales. In the discussion below, we focus on the 2-D fractal dimension of asphaltene aggregates although the results of the 3-D fractal dimension are also insightful, especially when the relations between 2-D and 3-D d_f are not well-established. The 2-D fractal dimension results show that there are two linear regions where the scaling relation $C(\epsilon) \sim \epsilon^{d_f}$ approximately holds: region 1 and region 2 shown in Figure 9. Region 1 represents nanoaggregate and associated clusters, which is a measure of the fractal dimension of the short-ranged parallel stacking of the aromatic rings, and region 2 represents aggregate clusters at the colloidal scale, which is a measure of the fractal dimension of the self-assembled network morphology.

Within region 1, the nanoaggregates formed by asphaltene A0 and A2 possess the relatively large fractal dimension of 1.85 and 1.87, respectively, indicating that they are short rod-like nanoaggregates, which is primarily attributed to the steric repulsions between the aliphatic side chains. The smaller fractal dimension (1.58) of nanoaggregates formed by the architecture A1 is due to the formation of longer rods by the stronger attractions between the larger aromatic rings, as has been observed in the snapshot shown in Figure 7. Within region 2, as expected, the fractal dimensions of all the

https://doi.org/10.1021/acs.langmuir.2c00323
Langmuir XXXX, XXX, XXX−XXX

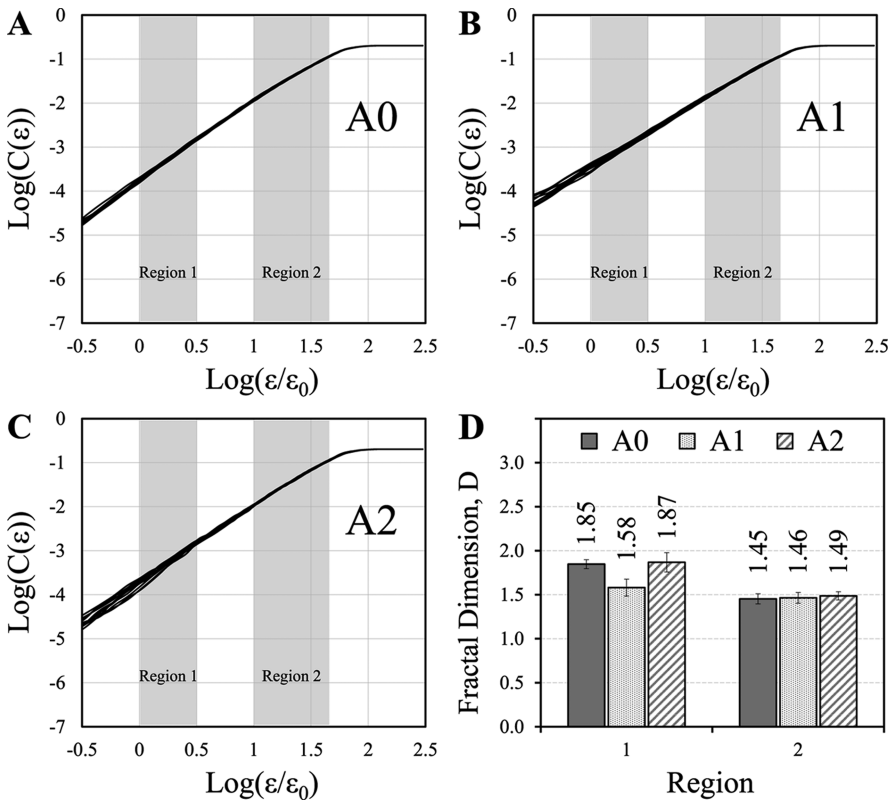

Figure 9. 2-D Fractal dimension of asphaltene molecules computed according to eq 2 *via* MD simulations, where (A) A0, (B) A1, and (C) A2 asphaltene molecules are dissolved in a mixture of toluene and *n*-heptane. In all simulations, the asphaltene mass fraction with respect to toluene is 15 wt % and T = 300 K. (D) Comparison of the average fractal dimension in region 1 and region 2 of the three studied systems. The reported values are the mean slope obtained from 100 independent configurations. Error bars are the standard deviations over those 100 slopes.

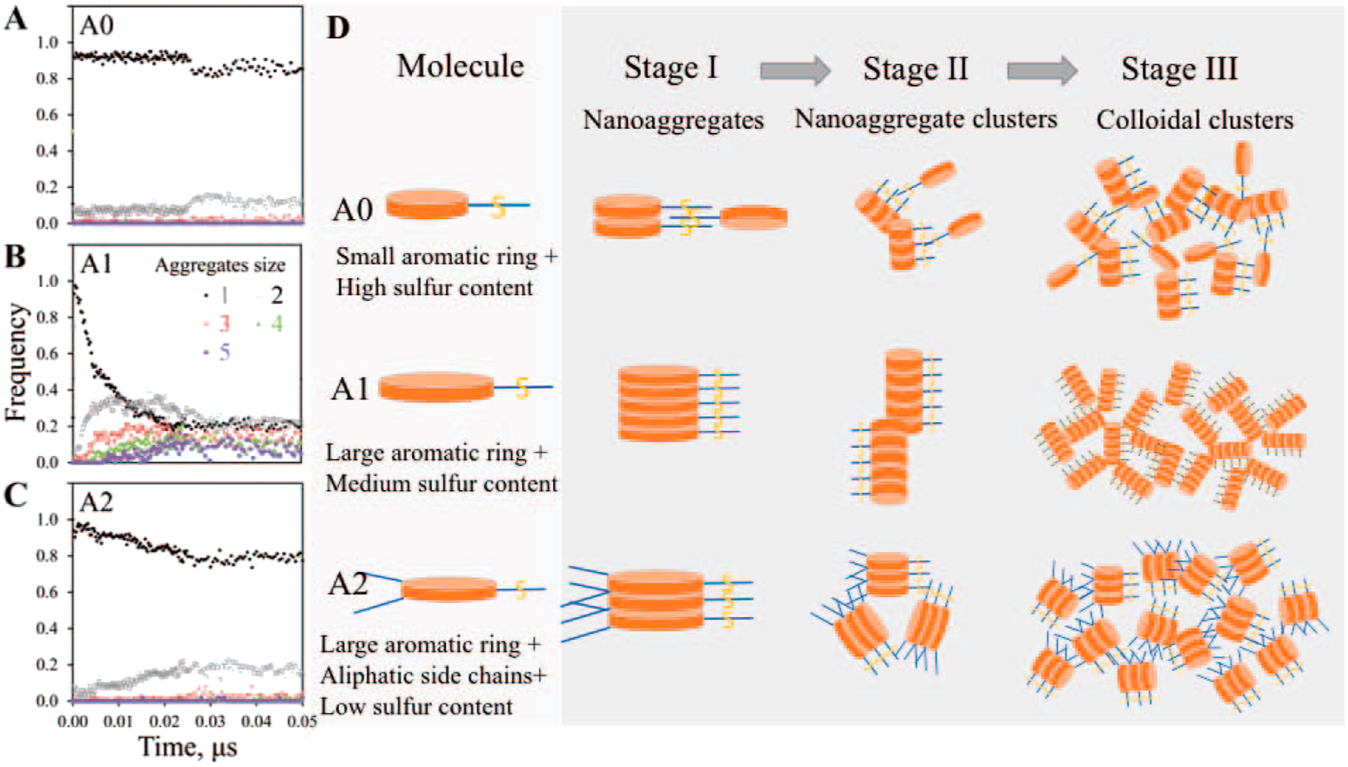

Figure 10. (A–C) Early-stage kinetics of aggregation of three model asphaltene molecules studied using molecular simulation. Aggregates of sizes 1, 2, 3, 4, and 5 are represented by black diamonds, grey squares, red asterisks, green triangles, and purple circles, respectively. (D) Schematic illustration of proposed effects of aliphatic sulfur on the three stages of asphaltene aggregation from three asphaltene molecules used in this study.

https://doi.org/10.1021/acs.langmuir.2c00323
Langmuir XXXX, XXX, XXX–XXX

aggregates are smaller than those observed in region 1, indicating that these colloidal aggregates are less compact and porous network structures, and their formation is largely governed by classic interaction potentials (*e.g.*, DLA and RLA). The fractal dimensions determined from these simulations are in acceptable agreement with our experimental results and other previous studies,[18,21,23,56] suggesting that sulfur-rich asphaltene aggregation at the colloidal scale can be generally described by an interaction potential, which is simply a summation of a short-range repulsive force, mainly originating from steric/electrostatic forces, and a long-range attractive force, primarily arising from Van der Waals dispersion forces. However, the specific mechanisms of how sulfur affects asphaltene aggregation at the colloidal scale depend on the structural features of the asphaltene molecules. For example, based on the discussion of the internal structure of aggregates, it is suggested that (1) A0 forms relatively small and noncompact aggregates largely due to its small aromatic core and electrostatic repulsion caused by the polar aliphatic sulfur and (2) A2 possess a large aromatic core, which is expected to form large and compact aggregates; however, it forms a similar aggregate structure as A0 does, indicating steric repulsion due to increased aliphatic side chains (no polar aliphatic sulfur) significantly reduces its aggregation tendency. In addition, slight deviations between experimental observations and theoretical simulations indicate that other nonclassical mechanisms might be considered in order to accurately predict sulfur-rich asphaltene aggregate formation.

General Effect of the Aliphatic Sulfur on Asphaltene Aggregation in This Study. We have studied the kinetics of the formation of asphaltene clusters in our simulations. Figure 10A−C shows how the aggregates of different sizes evolve over time in the three model asphaltene molecules. A0 does not have a significant tendency to aggregate, which is likely due to its small aromatic ring (Figure 10A). A1 shows a significant drop in clusters of size 1 (*i.e.*, unaggregated molecules), an initial increase in the number of clusters of size 2, and then a subsequent decrease in the size 2 clusters in favor of larger aggregates (Figure 10B). This result indicates that compared with a potential repulsion due to the polar aliphatic sulfur, the aromatic ring plays a dominant role in A1 aggregate formation. This is also in agreement with the physical picture that first, some small clusters form, which grow further to form larger clusters. A2, with a large aromatic ring, is expected to form large and compact aggregates; however, a slight drop of clusters of size 1 and a small increase in the size 2 cluster are observed, indicating steric repulsion likely due to increased aliphatic side chains (no polar aliphatic sulfur) significantly reduces its aggregation tendency (Figure 10C). Based on these simulation results plus our physical observations, we proposed a plausible mechanism that can be used to describe the general effect of sulfur on asphaltene aggregation in this study (Figure 10D): (I) at stage I, aliphatic sulfur has an important effect on the configurations/properties of nanoaggregates by means of noncovalent interactions (*e.g.*, Coulomb and/or van der Waals) with the side chain of neighbor molecules. This effect is most pronounced in sulfur-rich asphaltene with small aromatic cores (Figure 10A, D:A0). In this case, $\pi-\pi$, $\pi-\theta$, and $\theta-\theta$ interactions can result in nanoaggregates with short (small) rod-like shapes with noticeable variations. This effect is less pronounced for asphaltene with the same aliphatic sulfur while comprising large aromatic cores (Figure 10B,D:A1). In this case, $\pi-\pi$ interactions dominate aggregation and result in long (large) rod-like shape nanoaggregates, even though $\pi-\theta$ and $\theta-\theta$ interactions cannot be overlooked. When multiple nonpolar side chains interplay with aliphatic sulfur to prevent asphaltene aggregation, specific mechanisms, such as steric hindrance repulsion and electrostatic repulsion, need to be differentiated (Figure 10C,D:A2). In this case, although $\pi-\pi$ interactions due to large aromatic cores play an important role in the nanoaggregate structure, steric repulsion attributed to side chains limits the size of rod-like nanoaggregates. (II) At stage II, the nanoaggregates acting as primary particles form relatively small and compact clusters of nanoaggregates through the interactions between side chains. The morphology of the as-formed clusters is highly dependent on the polydispersity of nanoaggregates, which is partially attributed to the aliphatic sulfur. (III) At stage III, these submicron nanoaggregates clusters continue to diffuse, collide with each other, and form new aggregates until their sizes reach the threshold for sedimentation. The initial energy barrier caused by aliphatic sulfur and side chains likely corresponds to the RLA at the initial stage. As the cluster size grows, this energy barrier becomes less significant, and the aggregation mechanism converts to DLA.

CONCLUSIONS

The objective of this study is to quantify the growth kinetics and morphologies of colloidal aggregates formed from sulfur-rich asphaltenes and explore sulfur effects on this aggregation process, which remains poorly understood. Our experimental results generally show that the aggregate growth kinetics exhibit a crossover from RLA to DLA-like phenomena as the aggregation proceeds. The aggregation process is eventually controlled by DLA with an observed growth rate that is consistent with the Smoluchowski kinetics model. Structural results show that, despite a high degree of polydispersity, the aggregates display time-dependent self-similarity with a fractal dimension of 1.99 and 1.73, in accordance with those expected for RLA and DLA, respectively. These results illustrate the crucial relationship between dynamics and structure that is inherent in the kinetics of sulfur-rich asphaltene aggregate growth processes. These results also indicate that the nonclassical growth mechanisms should be quantified and correlated with classic growth mechanisms in future studies to help tune the overall properties of aggregates formed from sulfur-rich asphaltenes. Our simulation results show that aliphatic sulfur exerts interesting and nonmonotonic effects on the asphaltene aggregate formation from the nano-to micro-cluster scale. Specifically, interactions between aliphatic sulfur and the side chain of neighbor molecules account for the repulsive forces, which are attributed to the polydispersity in nanoaggregates and corresponding colloidal aggregates. For example, sulfur-rich asphaltenes, especially with small aromatic cores, tend to form nanoaggregates with short rod-like shapes, which eventually results in large aggregate clusters with polydisperse size distributions and slightly different fractal dimensions. These results could provide a valuable insight into existing oil refining efforts. For example, the repulsive interactions between asphaltene molecules originate from electrostatic forces and steric forces, which are largely controlled by the solvent quality (*e.g.*, a better solvent quality implies stronger repulsive forces, which prevent aggregation). Thus, using the asphaltene solubility or stability characteristics to scale the repulsive interactions in new solvent systems may be helpful. Furthermore, the findings from this work may have

https://doi.org/10.1021/acs.langmuir.2c00323
Langmuir XXXX, XXX, XXX−XXX

important implications for the transport and stability of NAPL contaminants in the environment. For instance, there is sufficient evidence suggesting that aggregate structure has important implications on their hydrodynamic properties, such as diffusion and deposition rate. In addition, the morphology and stability of aggregates affect the wettability of quartz minerals/sands, which could allow the NAPLs to penetrate/migrate into regions with smaller pore spaces (lower effective permeability), potentially contaminating previously clean aquifer and becoming less accessible to the flushing solutions. However, the extent to which aggregates formed from sulfur-rich asphaltenes affect NAPLs mobility and retention in porous media, especially under various environmental conditions, is still an open question. It is worth noting that this study is considered a proof of concept effort to demonstrate the feasibility of investigating the hierarchical asphaltene aggregation process by combining *in situ* microscopy and molecular simulation. More research is needed to explore the effects of key parameters (*e.g.*, solvent types, flow dynamics, and asphaltene concentrations) on this complex process.

■ ASSOCIATED CONTENT

Supporting Information

The Supporting Information is available free of charge at https://pubs.acs.org/doi/10.1021/acs.langmuir.2c00323.

> Autocorrelation Function; characterization of image objects as small and large clusters; weight percentage of the chemical composition for the surface and the bulk of the studied asphaltene sample; number of asphaltene and solvent molecules in simulations of multibody asphaltene aggregation; goodness of fit about the best fit of the characteristic time of asphaltene aggregation and fractal dimension of the aggregates formed; determination of the precipitation onset point from the microscopy method; plot of normalized autocorrelation against the distance of shift; definition and criteria of determination of clusters; Log−Log plot of the average area as a function of the radius of gyration of asphaltene nanoaggregates; size distribution and structural characteristics of nanoaggregates; snapshots of the MD simulations in equilibrium for the aromatic cores of A0 and A1; and 3-D fractal dimension of asphaltene aggregates computed according to eq 2 *via* MD simulations (PDF)

■ AUTHOR INFORMATION

Corresponding Author

Lei Wu − *Department of Civil Engineering, Ohio University, Athens, Ohio 45701, United States;* orcid.org/0000-0002-2781-7251; Phone: (740) 593-4771; Email: wul@ohio.edu

Authors

Christian B. Hammond − *Department of Civil Engineering, Ohio University, Athens, Ohio 45701, United States*

Mohammadreza Aghaaminiha − *Department of Civil Engineering, Ohio University, Athens, Ohio 45701, United States; Department of Chemical and Biomolecular Engineering, Ohio University, Athens, Ohio 45701, United States*

Sumit Sharma − *Department of Chemical and Biomolecular Engineering, Ohio University, Athens, Ohio 45701, United States;* orcid.org/0000-0003-3138-5487

Chongyang Shen − *Department of Soil and Water Sciences, China Agricultural University, Beijing 100193, China;* orcid.org/0000-0002-2517-3472

Hao Chen − *Department of Agriculture, University of Arkansas at Pine Bluff, Pine Bluff, Arkansas 71601, United States*

Complete contact information is available at: https://pubs.acs.org/10.1021/acs.langmuir.2c00323

Author Contributions

⊥C.B.H. and M.A. contributed equally to this work.

Notes

The authors declare no competing financial interest.

■ ACKNOWLEDGMENTS

L.W. would like to acknowledge the support of the National Science Foundation (NSF) grant 1836905. S.S. would like to acknowledge the support of the National Science Foundation (NSF) CAREER grant 2046095. Computational resources for this work are provided by the NSF XSEDE grant DMR190005 and the Ohio Supercomputer Center.

■ REFERENCES

(1) Durand, E.; Clemancey, M.; Lancelin, J.-M.; Verstraete, J.; Espinat, D.; Quoineaud, A.-A. Effect of chemical composition on asphaltenes aggregation. *Energy Fuels* **2010**, *24*, 1051−1062.

(2) Gray, M. R.; Tykwinski, R. R.; Stryker, J. M.; Tan, X. Supramolecular assembly model for aggregation of petroleum asphaltenes. *Energy Fuels* **2011**, *25*, 3125−3134.

(3) Almehaideb, R. A. Asphaltene precipitation and deposition in the near wellbore region: a modeling approach. *J. Petrol. Sci. Eng.* **2004**, *42*, 157−170.

(4) Hoepfner, M. P.; Fogler, H. S. Multiscale scattering investigations of asphaltene cluster breakup, nanoaggregate dissociation, and molecular ordering. *Langmuir* **2013**, *29*, 15423−15432.

(5) Mullins, O. C.; Seifert, D. J.; Zuo, J. Y.; Zeybek, M. Clusters of asphaltene nanoaggregates observed in oilfield reservoirs. *Energy Fuels* **2013**, *27*, 1752−1761.

(6) Bolouri, S. H.; Ghoodjani, E. Permeability impairment study due to asphaltene deposition: experimental and modeling approach. *Transport Porous Media* **2012**, *91*, 999−1012.

(7) Schutte, K. C. J.; Portela, L. M.; Twerda, A.; Henkes, R. A. W. M. Hydrodynamic perspective on asphaltene agglomeration and deposition. *Energy Fuels* **2015**, *29*, 2754−2767.

(8) Lin, Y.-J.; He, P.; Tavakkoli, M.; Mathew, N. T.; Fatt, Y. Y.; Chai, J. C.; Goharzadeh, A.; Vargas, F. M.; Biswal, S. L. Examining asphaltene solubility on deposition in model porous media. *Langmuir* **2016**, *32*, 8729−8734.

(9) Lin, Y.-J.; He, P.; Tavakkoli, M.; Mathew, N. T.; Fatt, Y. Y.; Chai, J. C.; Goharzadeh, A.; Vargas, F. M.; Biswal, S. L. Characterizing asphaltene deposition in the presence of chemical dispersants in porous media micromodels. *Energy Fuels* **2017**, *31*, 11660−11668.

(10) Zheng, J.; Behrens, S. H.; Borkovec, M.; Powers, S. E. Predicting the wettability of quartz surfaces exposed to dense nonaqueous phase liquids. *Environ. Sci. Technol.* **2001**, *35*, 2207−2213.

(11) Zheng, J.; Shao, J.; Powers, S. E. Asphaltenes from coal tar and creosote: Their role in reversing the wettability of aquifer systems. *J. Colloid Interface Sci.* **2001**, *244*, 365−371.

(12) Javanbakht, G.; Goual, L. Mobilization and micellar solubilization of NAPL contaminants in aquifer rocks. *J. Contam. Hydrol.* **2016**, *185*−*186*, 61−73.

(13) Javanbakht, G.; Goual, L. Impact of surfactant structure on napl mobilization and solubilization in porous media. *Ind. Eng. Chem. Res.* **2016**, *55*, 11736−11746.
(14) Lowry, E.; Sedghi, M.; Goual, L. Molecular simulations of NAPL removal from mineral surfaces using microemulsions and surfactants. *Colloids Surf., A* **2016**, *506*, 485−494.
(15) Pomerantz, A. E.; Seifert, D. J.; Bake, K. D.; Craddock, P. R.; Mullins, O. C.; Kodalen, B. G.; Mitra-Kirtley, S.; Bolin, T. B. Sulfur chemistry of asphaltenes from a highly compositionally graded oil column. *Energy Fuels* **2013**, *27*, 4604−4608.
(16) Rassamdana, H.; Dabir, B.; Nematy, M.; Farhani, M.; Sahimi, M. Asphalt flocculation and deposition: I. The onset of precipitation. *AIChE J.* **1996**, *42*, 10−22.
(17) Rassamdana, H.; Sahimi, M. Asphalt flocculation and deposition: II. Formation and growth of fractal aggregates. *AIChE J.* **1996**, *42*, 3318−3332.
(18) Yudin, I. K.; Nikolaenko, G. L.; Gorodetskii, E. E.; Kosov, V. I.; Melikyan, V. R.; Markhashov, E. L.; Frot, D.; Briolant, Y. Mechanisms of asphaltene aggregation in toluene−heptane mixtures. *J. Petrol. Sci. Eng.* **1998**, *20*, 297−301.
(19) Pacheco-Sánchez, J.; Zaragoza, I.; Martínez-Magadán, J. Asphaltene aggregation under vacuum at different temperatures by molecular dynamics. *Energy Fuels* **2003**, *17*, 1346−1355.
(20) Sodero, A. C. R.; Santos Silva, H.; Guevara Level, P.; Bouyssiere, B.; Korb, J.-P.; Carrier, H.; Alfarra, A.; Bégué, D.; Baraille, I. Investigation of the effect of sulfur heteroatom on asphaltene aggregation. *Energy Fuels* **2016**, *30*, 4758−4766.
(21) Hoepfner, M. P.; Vilas Bôas Fávero, C.; Haji-Akbari, N.; Fogler, H. S. The fractal aggregation of asphaltenes. *Langmuir* **2013**, *29*, 8799−8808.
(22) Tanaka, R.; Sato, E.; Hunt, J. E.; Winans, R. E.; Sato, S.; Takanohashi, T. Characterization of asphaltene aggregates using X-ray diffraction and small-angle X-ray scattering. *Energy Fuels* **2004**, *18*, 1118−1125.
(23) Wang, J.; Ferguson, A. L. Mesoscale simulation of asphaltene aggregation. *J. Phys. Chem. B* **2016**, *120*, 8016−8035.
(24) Roux, J.-N.; Broseta, D.; Demé, B. SANS study of asphaltene aggregation: concentration and solvent quality effects. *Langmuir* **2001**, *17*, 5085−5092.
(25) Headen, T. F.; Boek, E. S.; Stellbrink, J.; Scheven, U. M. Small angle neutron scattering (SANS and V-SANS) study of asphaltene aggregates in crude oil. *Langmuir* **2009**, *25*, 422−428.
(26) Hung, J.; Castillo, J.; Reyes, A. Kinetics of Asphaltene Aggregation in Toluene−Heptane Mixtures Studied By Confocal Microscopy. *Energy Fuels* **2005**, *19*, 898−904.
(27) Seifried, C. M.; Crawshaw, J.; Boek, E. S. Kinetics of asphaltene aggregation in crude oil studied by confocal laser-scanning microscopy. *Energy Fuels* **2013**, *27*, 1865−1872.
(28) Wu, G.; He, L.; Chen, D. Sorption and distribution of asphaltene, resin, aromatic and saturate fractions of heavy crude oil on quartz surface: molecular dynamic simulation. *Chemosphere* **2013**, *92*, 1465−1471.
(29) Marrink, S. J.; Risselada, H. J.; Yefimov, S.; Tieleman, D. P.; De Vries, A. H. The MARTINI force field: coarse grained model for biomolecular simulations. *J. Phys. Chem. B* **2007**, *111*, 7812−7824.
(30) Jover, J. F.; Müller, E. A.; Haslam, A. J.; Galindo, A.; Jackson, G.; Toulhoat, H.; Nieto-Draghi, C. Aspects of asphaltene aggregation obtained from coarse-grained molecular modeling. *Energy Fuels* **2015**, *29*, 556−566.
(31) Zaluzec, N. J.; Janssen, A.; Kulzick, M. A.; Burke, M. G. In situ Analytical Microscopy of Asphaltene Aggregation and Growth. *Microsc. Microanal.* **2017**, *23*, 932−933.
(32) Eyssautier, J.; Frot, D.; Barré, L. Structure and dynamic properties of colloidal asphaltene aggregates. *Langmuir* **2012**, *28*, 11997−12004.
(33) Meakin, P. Formation of fractal clusters and networks by irreversible diffusion-limited aggregation. *Phys. Rev. Lett.* **1983**, *51*, 1119.
(34) Meakin, P.; Family, F. Structure and dynamics of reaction-limited aggregation. *Phys. Rev. A* **1987**, *36*, 5498.
(35) Haji-Akbari, N.; Teeraphapkul, P.; Fogler, H. S. Effect of asphaltene concentration on the aggregation and precipitation tendency of asphaltenes. *Energy Fuels* **2014**, *28*, 909−919.
(36) Wu, L.; Ortiz, C.; Xu, Y.; Willenbring, J.; Jerolmack, D. In situ liquid cell observations of asbestos fiber diffusion in water. *Environ. Sci. Technol.* **2015**, *49*, 13340−13349.
(37) Wu, L.; Ortiz, C. P.; Jerolmack, D. J. Aggregation of elongated colloids in water. *Langmuir* **2017**, *33*, 622−629.
(38) Bussi, G.; Donadio, D.; Parrinello, M. Canonical sampling through velocity rescaling. *J. Chem. Phys.* **2007**, *126*, 014101.
(39) Abraham, M. J.; Murtola, T.; Schulz, R.; Páll, S.; Smith, J. C.; Hess, B.; Lindahl, E. GROMACS: High performance molecular simulations through multi-level parallelism from laptops to supercomputers. *SoftwareX* **2015**, *1−2*, 19−25.
(40) Ingólfsson, H. I.; Melo, M. N.; Van Eerden, F. J.; Arnarez, C.; Lopez, C. A.; Wassenaar, T. A.; Periole, X.; De Vries, A. H.; Tieleman, D. P.; Marrink, S. J. Lipid organization of the plasma membrane. *J. Am. Chem. Soc.* **2014**, *136*, 14554−14559.
(41) Aghaaminiha, M.; Farnoud, A. M.; Sharma, S. Quantitative relationship between cholesterol distribution and ordering of lipids in asymmetric lipid bilayers. *Soft Matter* **2021**, *17*, 2742−2752.
(42) Bava, Y. B.; Geronés, M.; Giovanetti, L. J.; Andrini, L.; Erben, M. F. Speciation of sulphur in asphaltenes and resins from Argentinian petroleum by using XANES spectroscopy. *Fuel* **2019**, *256*, 115952.
(43) Waldo, G. S.; Mullins, O. C.; Penner-Hahn, J. E.; Cramer, S. P. Determination of the chemical environment of sulphur in petroleum asphaltenes by X-ray absorption spectroscopy. *Fuel* **1992**, *71*, 53−57.
(44) Guzmán, H. J.; Isquierdo, F.; Carbognani, L.; Vitale, G.; Scott, C. E.; Pereira-Almao, P. X-ray photoelectron spectroscopy analysis of hydrotreated athabasca asphaltenes. *Energy Fuels* **2017**, *31*, 10706−10717.
(45) Kelemen, S. R.; George, G. N.; Gorbaty, M. L. Direct determination and quantification of sulphur forms in heavy petroleum and coals. *Fuel* **1990**, *69*, 939−944.
(46) Littlejohn, D.; Chang, S.-G. An XPS study of nitrogen-sulfur compounds. *J. Electron Spectrosc. Relat. Phenom.* **1995**, *71*, 47−50.
(47) Lindberg, B. J.; Hamrin, K.; Johansson, G.; Gelius, U.; Fahlman, A.; Nordling, C.; Siegbahn, K. Molecular spectroscopy by means of ESCA II. Sulfur compounds. Correlation of electron binding energy with structure. *Phys. Scr.* **1970**, *1*, 286.
(48) Grzybek, T.; Pietrzak, R.; Wachowska, H. The comparison of oxygen and sulfur species formed by coal oxidation with O2/Na2CO3 or peroxyacetic acid solution. XPS studies. *Energy Fuels* **2004**, *18*, 804−809.
(49) Sholl, D. S.; Skodje, R. T. Late-stage coarsening of adlayers by dynamic cluster coalescence. *Phys. A* **1996**, *231*, 631−647.
(50) Sheu, E. Y.; Liang, K. S.; Sinha, S. K.; Overfield, R. E. Polydispersity analysis of asphaltene solutions in toluene. *J. Colloid Interface Sci.* **1992**, *153*, 399−410.
(51) Trejo, F.; Ancheyta, J.; Rana, M. S. Structural characterization of asphaltenes obtained from hydroprocessed crude oils by SEM and TEM. *Energy Fuels* **2009**, *23*, 429−439.
(52) Rahmani, N. H. G.; Dabros, T.; Masliyah, J. H. Fractal structure of asphaltene aggregates. *J. Colloid Interface Sci.* **2005**, *285*, 599−608.
(53) Gmachowski, L.; Paczuski, M. Fractal dimension of asphaltene aggregates determined by turbidity. *Colloids Surf., A* **2011**, *384*, 461−465.
(54) Hammond, C. B.; Wang, D.; Wu, L. Precipitant Effects on Aggregates Structure of Asphaltene and Their Implications for Groundwater Remediation. *Water* **2020**, *12*, 2116.
(55) Javanbakht, G.; Sedghi, M.; Welch, W. R. W.; Goual, L.; Hoepfner, M. P. Molecular polydispersity improves prediction of asphaltene aggregation. *J. Mol. Liq.* **2018**, *256*, 382−394.
(56) Ahmadi, M.; Hassanzadeh, H.; Abedi, J. Asphaltene Mesoscale Aggregation Behavior in Organic Solvents-A Brownian Dynamics Study. *J. Phys. Chem. B* **2018**, *122*, 8477−8492.

https://doi.org/10.1021/acs.langmuir.2c00323
Langmuir XXXX, XXX, XXX−XXX

(57) Woehl, T. J.; Park, C.; Evans, J. E.; Arslan, I.; Ristenpart, W. D.; Browning, N. D. Direct observation of aggregative nanoparticle growth: Kinetic modeling of the size distribution and growth rate. *Nano Lett.* **2014**, *14*, 373−378.

https://doi.org/10.1021/acs.langmuir.2c00323
Langmuir XXXX, XXX, XXX−XXX